Millimeter Wave Channel Measurements and Modelling in an Indoor Hotspot Scenario at 28 GHz

Pan Tang*, Jianhua Zhang*, Mansoor Shafi†, Pawel A. Dmochowski‡, Peter J. Smith§
* State Key Lab of Networking and Switching Technology, Beijing University of Posts and Telecommunications
† Spark New Zealand, Wellington, New Zealand
‡ School of Engineering and Computer Science, Victoria University of Wellington, Wellington, New Zealand
§ School of Mathematics and Statistics, Victoria University of Wellington, Wellington, New Zealand
{tangpan27, jhzhang,}@bupt.edu.cn, mansoor.shafi@spark.co.nz, pawel.dmochowski@ecs.vuw.ac.nz, peter.smith@msor.vuw.ac.nz

***Abstract*—Millimeter-wave channel models are fundamental for evaluating the performance of technologies for 5G. In this paper, we present two kinds of millimeter-wave channel measurements, fixed point measurements and virtual measurements, in an indoor open office. A correlation sounder with a bandwidth of 600 MHz is used to carry out these measurements. Then, channel parameters, e.g., the path loss, shadow fading, root mean square (RMS) delay spread (DS), K-factor, delay-cluster number and angular spread, are extracted and modelled. These extracted models will enable the generation of an impulse response for the indoor hotspot environment. Differences between our measurement-based channel model parameters and the International Telecommunication Union (ITU) channel model are discussed. The impact of differences on capacity are investigated by simulations. We find that the ITU channel model is optimistic about capacity. These results can help researchers to use millimeter-wave channel models for indoor office scenarios when evaluating 5G performance.**

I. Introduction

Motivated by the spectrum needs of 5G [1], [2], there is considerable a large interest in studying the propagation characteristics of millimeter wave bands. Many different groups around the world have embarked on producing millimeter-wave channel models, such as the 3rd Generation Partnership Project (3GPP) (for 0.5-100 GHz) [3], International Telecommunication Union (ITU) (for 0.5-100 GHz) [4], the Mobile and Wireless Communications Enablers for the Twenty-Twenty Information Society (METIS) (up to 70 GHz for a stochastic model, and up to 100 GHz for a map-based model) [5], 5G millimeter-wave Channel Model Alliance (for 0.5-100 GHz) [6], NYU WIRELESS (for 0.5-100 GHz) [7]. Standardized channel models to study the performance of 5G systems have been published by the 3GPP and ITU [3], [4]. The Globecom white paper for 5G defined some typical deployment scenarios, e.g., indoor (InH) open and closed office, shopping malls, and gave a part of channel parameters for the indoor office [8].

An accurate characterization of radio propagation is important to predict real world performance of radio systems. Measurements and models for path loss and small scale fading for indoor scenarios are given in [9], [10] and [11]–[13], respectively. In this paper we measure both the large and small fading characteristics for a typical indoor office layout. We then derive 3GPP/ITU model parameters of the impulse response. The path loss in the 3GPP/ITU models is based on a floating intercept model, known as the alpha-beta-gamma (ABG) model [3] and the clusters are characterized by a joint delay-angle probability density function, such that a group of traveling multipaths departs and arrives from a unique angle of departure (AoD)-angle of arrival (AoA) combination centered around a mean propagation delay [3]. The cluster number in the 3GPP model is assumed constant and is the same as that for microwave bands [3]. We also derive where possible the NYUSIM based model parameters. The path loss in the NYUSIM model [14] is a close-in (CI) free space intercept model and the clusters use time cluster (TC) and spatial lobe (SL) concepts to describe multipath behavior [14]. The cluster number in the NYUSIM model is a Poisson random variable with a mean value that reflects the sparsity of the millimeter-wave channel. The contributions of this paper are:

- Millimeter-wave channel measurements for a typical indoor office are presented. Note that the indoor office is a genuine, operational workspace in a typical central business district (CBD) office building. We provide models for path loss, shadowing, RMS delay spread, Ricean K-factor, delay-cluster numbers and angular spread in azimuth and elevation.
- For many of the above parameters we model their statistical properties by an appropriate distribution (mostly similar to 3GPP) and provide the parameter values. We compare the results with that shown in other literature and [4]. Differences between our measurements and the standardized models are then investigated.
- We use our model and the standardized model [4] to generate a channel impulse response and then compare the ergodic capacity obtained from both. We find that ergodic capacity calculated based on our models is smaller as [4] assumes a richer multipath structure (cluster numbers) than that found in our measurements. The above measurements are now standardized as the indoor hotspot optional model I in the ITU [4].

II. Measurement Setup

A wideband correlation sounder with a bandwidth of 600 MHz was used to capture the channel information at the central frequency of 28 GHz. A pseudo-random noise sequence (511 chips) was generated by the baseband-signal generator as a

probing signal with a chip rate of 400 MHz and a pulse repetition interval of 1277.5 ns. The signal was up-converted to 28 GHz and passed through an amplifier with a 1 dB compression point of 33 dBm and a gain of 56 dB. The maximum output power was 30 dBm. The receiver (RX) utilized a low noise amplifier with a 1 dB compression point of 10 dBm and a gain of 50 dB prior to down-conversion to baseband. The receiver module stored the IQ data in real time. Table I shows the parameters of the three kinds of antennas used. Two types of measurements were conducted

TABLE I
ANTENNA PARAMETERS

Antenna types	Biconical/Sectored/Horn
Antenna gain	2.93 dBi/9.4 dBi/25 dBi
Antenna polarization	Vertical
Antenna azimuth HPBW	$360°/92.19°/10°$
Antenna elevation HPBW	$40°/40.15°/11°$
Antenna height	1.75 m

in the indoor office. Fixed-point measurements were used to obtain path loss, shadow fading, RMS DS, K-factor and delay-cluster number. Here, two omnidirectional biconical-antennas ($360°$ and $40°$ half-power-beam-widths (HPBW) in azimuth and elevation, respectively) at TX and RX sides were used to obtain 1000 channel impulse responses (CIRs) at each position. During the fixed-pointed measurements, antennas were kept still. The second type of measurement was the virtual measurement, in which a horn antenna was rotated to simulate an antenna array. This was used to obtain the angular spread. It used an omnidirectional biconical-antenna at the TX side while a directional horn-antenna ($10°$ and $11°$ HPBW in azimuth and elevation, respectively) was mounted in an electrical positioner at the RX side, which allowed for horizontal antenna rotation and vertical tilts with $1°$ accuracy. The TX antenna was fixed and the RX antenna was rotated in steps of $10°$ in azimuth from $0°$ to $360°$ at elevation angles of $-10°$, $0°$, and $10°$. To obtain both arrival and departure angle measurements, the TX and RX positions were interchanged. Each horn-antenna pointing direction recorded 1000 CIR measurements. Two different pairs of antennas were used. For the fixed-point measurement, the omnidirectional antenna can almost capture all MPCs in the channel so that each omnidirectional CIR sample contains information of the whole channel. However, the directional CIR samples obtained by the horn antenna in virtual measurements are the superposition of only the MPCs within the narrow HPBW. We can use these directional CIR samples with different angle information to estimate the angular characteristics of channels.

Fig. 1 shows the measurement layout. The fixed-point measurements in the open office included 70 positions (30 line-of-sight (LoS) positions and 40 (non-line-of-sight) (NLoS) positions), of which 10 LoS positions and 9 NLoS positions were selected to carry out virtual measurements.

III. CHANNEL MODELS

The ITU model is proposed based on many measurements from different research groups and provides a good reference for researchers. Based on our measurements, we can extract

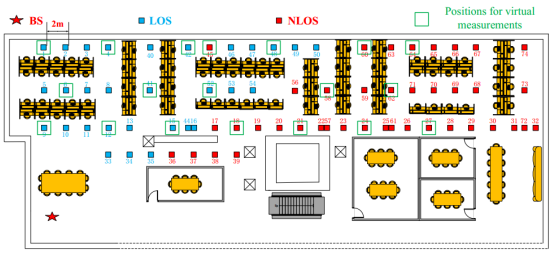

Fig. 1. The measurement layout in the indoor open office.

channel parameters to fit the 3GPP style channel model. In the following text, we show the results of estimating these channel parameters.

A. Path loss and shadow fading

In each measured position, 1000 samples of path loss are obtained from the fixed-point measurements and the floating-intercept (FI) model is used to model the path loss as follows:

$$PL_{FI}[dB](d) = \beta + 10\alpha \log_{10} d + X_{\sigma}^{FI}, \tag{1}$$

where β and α are two parameters of fit, and X_{σ} is a zero-mean Gaussian variable representing the shadowing. This model has been adopted in channel standardizations, e.g., WINNER II and 3GPP channel models [3]. In [10], the CI path loss model was discussed and given by

$$PL_{CI}(f,d)[dB] = 20\log_{10}\left(\frac{4\pi d_0 f}{c}\right) + 10 n_{CI} \log_{10}\left(\frac{d}{d_0}\right) + X_{\sigma}^{CI} \quad \text{for } d \geq d_0, d_0 = 1m, \tag{2}$$

where d_0 is the received-power reference point, which is typically chosen to be 1m, f is the frequency, c is the speed of light, and n_{CI} is the path loss exponent (PLE). The CI path loss model is a function of frequency and is simpler than the FI model having only one parameter. Here, we consider both models and the corresponding parameters are obtained by a minimum-mean-square-error (MMSE) fit.

The path loss fitting results for both models in LoS and NLoS scenarios are shown in Fig. 2. In LoS scenarios, the path loss obtained from measurements is smaller than the free space path loss. This can be explained by the fact that many multiple path components (MPCs), e.g., reflected paths, scattered paths, are received by the receiver due to the confined space. However, in NLoS scenarios, the dominant (i.e., LoS) path, is obstructed by walls and results in higher path loss. The measured path loss exponent (PLE) values in the CI model are 1.45 for LoS scenarios and 2.18 for NLoS scenarios, which are smaller than the ITU channel model values for indoor hotspot scenarios (see Table II). In [15], measurement results in an office at 28 GHz were presented and smaller PLEs (1.1 for LoS scenarios and 2.7 for NLoS scenarios) were also obtained. We also plot measured results with the FI model in Fig. 2 and these are almost overlapped with the CI model.

B. RMS DS

RMS DS describes the time dispersion of MPCs, and can be used to calculate the coherence bandwidth. For a wideband channel, the receiver can resolve multiple paths according

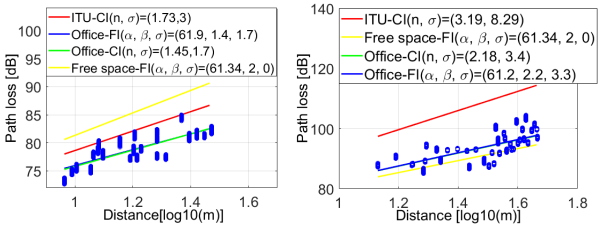

(a) LoS (b) NLoS

Fig. 2. Path loss results in the indoor open office.

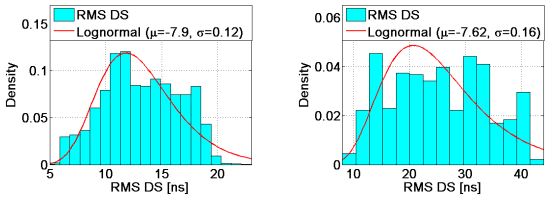

(a) LoS (b) NLoS

Fig. 3. Statistical results for RMS DS in the indoor open office.

to their delay and the CIR is commonly represented by the superposition of many plane waves as follows:

$$h(t,\tau) = V\delta(\tau-\tau_0) + \sum_{l=1}^{L} a_l \exp(j(2\pi f_{max}\cos(\vartheta_l)t + \varphi_l))\delta(\tau-\tau_l), \quad (3)$$

where the complex constant, V, represents the deterministic (typically LoS) component with excess delay τ_0 and $|V| = a_0$. a_l, τ_l, ϑ_l and φ_l are the amplitude, excess delay, arrival angle and initial phase of the l-th stochastic (typically reflected) component, respectively. L is the number of all MPCs. f_{max} represents the maximum Doppler shift.

Here, we study the statistics of the RMS DS based on the fixed-point measured data. Fig. 3 shows the results for RMS DS. The lognormal distribution is used to fit the RMS DS, and μ is -7.9 ($10^{-7.9}\cdot 10^9 \approx 12.59\ ns$) for LoS scenarios and -7.62 ($10^{-7.62}\cdot 10^9 \approx 23.99\ ns$) for NLoS scenarios. In [16], the mean value of the RMS DS in a open office is 12 ns for LoS scenarios, which is similar to our results. However, these results are smaller than that both for LoS and NLoS scenarios in the ITU model shown in Table II.

C. K-factor

The K-factor is a measure of severity of small scale fading and is defined as the ratio of the power of the deterministic MPC and the power of all other stochastic MPCs. Thus, we can obtain the K-factor in linear scale according to (3) as

$$K = \frac{|V|^2}{\sum_{l=1}^{L}|a_l|^2}. \quad (4)$$

Here, we apply the moment method [17] to estimate the K-factor. Note that there is no mobility in our measurements, i.e., temporal variation does not occur. Commonly, the moment-method is used to extract the K-factor over time-varying samples. However, in [18], the K-factor was investigated across different frequencies. Thus, we have applied the moment-method [17] to estimate the K-factor based upon the analysis of frequency-selectivity. The transfer function can be expressed as follows:

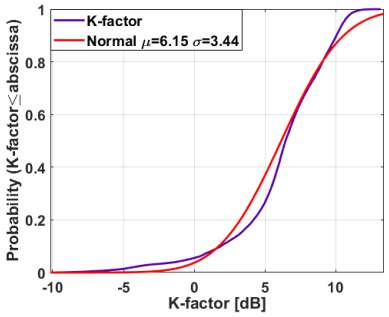

Fig. 4. Statistical results for the K-factor in the indoor open office.

$$H(f) = V\exp(-j2\pi f\tau_0) + \sum_{l=1}^{L} a_l \exp(j(2\pi f_{max}\cos(\vartheta_l)t + \varphi_l - 2\pi f\tau_l)). \quad (5)$$

If L is big enough and the measured 3dB-bandwidth is wide enough, according to the central limit theorem, we can assume $H(f) \backsim \mathcal{CN}(V\exp(-j2\pi\tau_0), \sum_{l=1}^{L}|a_l|^2)$. Then, $|H(f)|^2$ can be considered as the power gain G to calculate the K-factor.

Fig. 4 shows the lognormal fitting results to the cumulative distribution function (CDF) of the K-factor in dB in the indoor open office. The mean value of the K-factor is 6.15 dB. In [19], the K-factor ranges from 9 dB to 15 dB for LoS scenarios while it ranges from 5 dB to 8 dB for NLoS scenarios in the outdoor measurements, and the measured distance is from 8 m to 12.9 m. We can say that for the close distance and open environment, stochastic components account for a smaller portion of the received power.

D. The cluster characteristics in delay domain

In [20], a statistical spatial channel model (SSCM) is presented based on a time cluster, spatial lobe (TCSL) approach. This model is different to the cluster delay line (CDL) model, in which clustering is done in both delay and angular domains. Here, we also show clustering characteristics in the delay domain. The K-means algorithm is a common computational approach [21] and provides a framework for automatic clustering based on the K-means algorithm using the power of MPCs to weight the multiple component distance (MCD). Further improvements to this approach include are given in [22] and [23] which are used here. Note that only one component, the delay, is used to calculate the MCD. Figs. 5 shows results for the mean cluster numbers in the delay domain in the indoor open office and a Poisson model is used [20]. We observe that the mean cluster numbers are 4 (LoS) and 6 (NLoS) for the indoor open office. These results differ to those in [20], with more delay clusters found in our measurements, but still confirm the sparsity of the millimeter-wave channel. Furthermore, the delay cluster number in LoS scenarios is less than that in NLoS scenarios. The statistical results for cluster RMS DS are also calculated here, which describe the delay dispersion within a cluster. For reasons of space, no figures are shown here but the fitted parameters are shown in Table II. It should be noted that the cluster RMS DS for NLoS scenarios in the indoor open office is smaller than that for LoS. This means that in the NLoS scenarios, the MPCs in a cluster are more similar in the delay domain.

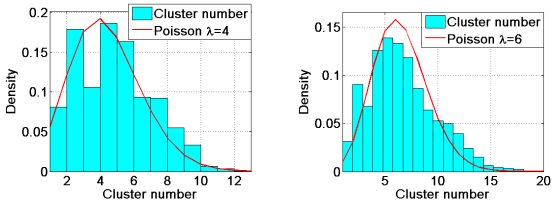

(a) LoS (b) NLoS

Fig. 5. Statistical results for the cluster numbers in the delay domain.

E. Angular characteristics

In each measured position, we obtain 72×3 groups of CIRs and the space-alternating generalized expectation-maximization (SAGE) algorithm [24] is used to jointly estimate the angular spread of arrival and departure both in azimuth and elevation domains. The received signal for NLoS scenarios at the i-th pointing angle of the horn antenna can be written as:

$$s_i(t) = \sum_{l}^{L} a_l F_i(\phi_l, \theta_l)\delta(t, \tau_l) + w_i(t), \quad l = 0, ...L, \quad (6)$$

where $a_l, \phi_l, \theta_l, \tau_l$ denote the complex attenuation, azimuth angle of arrival, elevation angle of arrival and delay of the l-th path, respectively. $w_i(t)$ is complex additive white Gaussian noise, $F_i(\phi_l, \theta_l)$ is the receiver antenna response at the i-th pointing angle. ϕ_l and θ_l are the azimuth angle and elevation angle of the l-th MPC, respectively. The SAGE algorithm is based on the maximum-likelihood criterion and can extract the channel parameters, $[a_l, \phi_l, \theta_l, \tau_l]$, from received signals. Firstly, these parameters are initialized as $[a_l^{'}, \phi_l^{'}, \theta_l^{'}, \tau_l^{'}]$. Then, these parameters are updated sequentially using:

$$\begin{aligned}\tau_l^{''} &= \text{argmax}_{\tau_l} z(a_l^{'}, \phi_l^{'}, \theta_l^{'}, \tau_l^{'}); \phi_l^{''} = \text{argmax}_{\phi_l} z(a_l^{'}, \phi_l^{'}, \theta_l^{'}, \tau_l^{''}) \\ \theta_l^{''} &= \text{argmax}_{\theta_l} z(a_l^{'}, \phi_l^{''}, \theta_l^{'}, \tau_l^{''}); a_l^{''} = \text{argmax}_{a_l} z(a_l^{'}, \phi_l^{'}, \theta_l^{'}, \tau_l^{'}),\end{aligned} \quad (7)$$

where $z(\cdot)$ is a part of the log-likelihood function that is used to find the maximum likelihood values [24]. After convergence, we obtain the final estimated channel parameters. The fitted results for RMS angular spread are shown in Fig. 6 and Fig. 7 using a lognormal distribution as in the ITU channel model. The results in Fig. 7(a) do not show a good fit. This may be because the virtual measurement positions are limited and some MPCs with small azimuth spreads of arrival are not captured. Generally, we can see that the angular spread in the azimuth domain is larger than that in the elevation domain. Furthermore, we see that the measured values of RMS angular spreads, including ASA, ASD, ZSA, are all smaller than the ITU values shown in Table II. For example, μ_{lgASA} in the indoor open office is 1.15 ($10^{1.15} \approx 14.13°$) while it is 1.5 ($10^{1.5} \approx 31.62°$) in the ITU channel model for indoor hotspot scenarios, see Table II. These differences indicate that any particular location may well be different to the typical scenarios embodied in the ITU model, and, especially for millimeter-wave bands, the channel parameters are sensitive to the environment.

IV. Parameter Differences and Channel Capacity

Finally, we compare the measured parameter values to those specified by [4], as listed in Table II. In Fig. 8 we evaluate the single user ergodic capacity for a link with 256

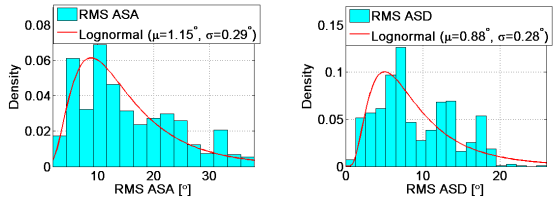

(a) ASA (b) ASD

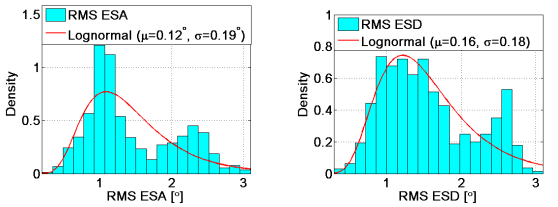

(c) ESA (d) ESD

Fig. 6. Fitted values of the RMS AS for LoS scenarios.

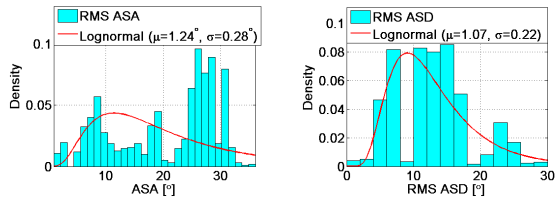

(a) ASA (b) ASD

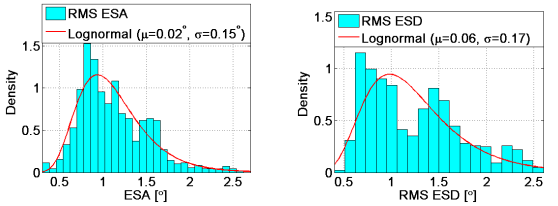

(c) ESA (d) ESD

Fig. 7. Fitted values of the RMS AS for NLoS scenarios.

antennas base station and 4 mobile-station antennas operating at 28 GHz. The antenna numbers are chosen according to [4]. The figure shows the performance predicted by the ITU Indoor Hotspot-A scenario, as well as that obtained using the measured parameter values. The parameters not obtained by the measurement campaign were set to those specified by the ITU model. We observe that the ITU model results in a higher predicted ergodic capacity (equivalent to a 6.59 dB gain at a signal noise ratio (SNR) of 20 dB). This is mainly because the ITU model has larger number of assumed clusters [14] and multipath richness.

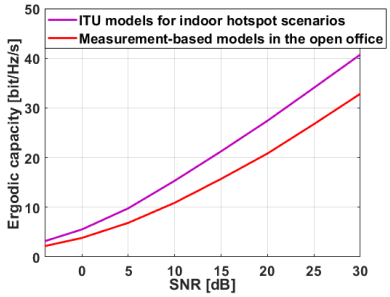

Fig. 8. The ergodic capacity for ITU indoor model and our measurements for a 256 x 4 single user case.

[1]Clustering is done in the delay domain in our analysis so that those two parameters should be delay-cluster number and delay cluster RMS DS.

TABLE II
THE CHANNEL MODEL PARAMETERS FOR INDOOR ENVIRONMENTS. THE MEASUREMENT-BASED MODEL PARAMETERS ARE EXTRACTED FROM OUR INDOOR OPEN OFFICE MEASUREMENTS SHOWN IN SECTION II.

Scenarios		Measurement-based		ITU channel models at 28 GHz			
		Indoor open office		Indoor hotspot-A		Indoor hotspot-B	
		LoS	NLoS	LoS	NLoS	LoS	NLoS
PL_{CI}	n	1.45	2.18	1.73	3.19	1.73	3.19
	σ	1.7	3.4	3	8.29	3	8.29
PL_{FI}	α	61.9	61.2	N/A	53.33	N/A	53.33
	β	1.4	2.2	N/A	3.83	N/A	3.83
	σ	1.7	3.3	N/A	8.03	N/A	8.03
Log_{10}(DS/1s)	μ_{lgDS}	-7.9	-7.62	-7.7	-7.58	-7.71	-7.58
	σ_{lgDS}	0.12	0.16	0.18	0.2	0.18	0.2
Log_{10}(ASD/1°)	μ_{lgASD}	0.88	1.07	1.6	1.62	1.6	1.62
	σ_{lgASD}	0.28	0.22	0.18	0.25	0.18	0.25
Log_{10}(ASA/1°)	μ_{lgASA}	1.15	1.24	1.5	1.7	1.5	1.7
	σ_{lgASA}	0.29	0.28	0.29	0.23	0.23	0.23
Log_{10}(ZSD/1°)	μ_{lgZSD}	0.16	0.06	0.14	1.08	0.14	1.08
	σ_{lgZSD}	0.18	0.17	0.49	0.36	0.49	0.36
Log_{10}(ZSA/1°)	μ_{lgZSA}	0.12	0.02	1.06	1.17	1.06	1.17
	σ_{lgZSA}	0.19	0.15	0.21	0.61	0.21	0.61
K [dB]	μ_K	6.15	N/A	7	N/A	7	N/A
	σ_K	3.44	N/A	4	N/A	4	N/A
Cluster number[1]		4	6	15	19	15	19
Cluster RMS DS[1]		5.93	4.97	N/A	N/A	N/A	N/A

V. CONCLUSION

We have presented the results of millimeter-wave channel measurements for a typical indoor office at 28 GHz. Fixed-point and virtual measurements were used to obtain path loss, shadow fading, RMS DS, RMS AS and delay-cluster numbers. The results were compared against parameter values specified by the ITU channel model, including the impact on the predicted channel capacity. We identified the differences between our measurement-based model parameters and the ITU model. For example, the cluster numbers are 4 (LoS) and 6 (NLoS) in our measurement-based model, which are smaller than that in the ITU model. In turn these differences result in different capacity.

ACKNOWLEDGMENT

The work of the Chinese authors is supported by the National Natural Science Foundation of China (Grant No. 61322110), the National Science and Technology Major Project of the Ministry of Science and Technology (Grant No. 2017ZX03001028-003).

REFERENCES

[1] M. Shafi et al., "5G: a tutorial overview of standards, trials, challenges, deployment, and practice," IEEE Journal on Selected Areas in Communications, vol. 35, no. 6, pp. 1201-1221, Jun. 2017.

[2] J. Zhang et al., "6C100 GHz research progress and challenges from a channel perspective for fifth generation (5G) and future wireless communication." Science China Information Sciences 60.8 (2017): 080301.

[3] "3GPP TR 38.901 V14.1.1 technical report: study on channel model for frequency spectrum above 6 GHz (release 14.1.1)," July 2017.

[4] ITU-R M.2412-0, "Guidelines for evaluation of radio interface technologies for IMT-2020," International Telecommunications Union (ITU), Oct. 2017.

[5] V. Nurmela et al., "METIS channel models," FP7 METIS, Deliverable D, vol. 1, 2015.

[6] NIST. [Online]. Available: http://www.nist.gov/ctl/wireless-networks/5gmillimeterwavechannelmodel.cfm.

[7] S. Sun et al., "A novel millimeter-wave channel simulator and applications for 5G wireless communications," in 2017 IEEE International Conference on Communications (ICC), Paris, France, 2017, pp. 1-7.

[8] 5GCMSIG. [Online]: http://www.5gworkshops.com/5GCM.html.

[9] J. Zhu et al., "Large-scale fading characteristics of indoor channel at 45-GHz band," in IEEE Antennas and Wireless Propagation Letters, vol. 14, pp. 735-738, 2015.

[10] G. R. MacCartney et al., "Indoor office wideband millimeter-wave propagation measurements and channel models at 28 and 73 GHz for ultra-dense 5G wireless networks," IEEE Access, vol. 3, pp. 2388-2424, 2015.

[11] J. Ko et al., "Millimeter-wave channel measurements and analysis for statistical spatial channel model in in-building and urban environments at 28 GHz," in IEEE Transactions on Wireless Communications, vol. 16, no. 9, pp. 5853-5868, Sept. 2017.

[12] X. Wu et al., "60-GHz millimeter-wave channel measurements and modeling for indoor office environments," in IEEE Transactions on Antennas and Propagation, vol. 65, no. 4, pp. 1912-1924, April 2017.

[13] X. Yin et al., "Experimental multipath-cluster characteristics of 28-GHz propagation channel," in IEEE Access, vol. 3, pp. 3138-3150, 2015.

[14] T. S. Rappaport et al., "Investigation and comparison of 3GPP and NYUSIM channel models for 5G wireless communications," in 2017 IEEE 86th Vehicular Technology Conference (VTC-Fall), Sep. 2017.

[15] S. Deng et al., "28 GHz and 73 GHz millimeter-wave indoor propagation measurements and path loss models," in 2015 IEEE International Conference on Communication Workshop (ICCW), 2015, pp. 1244-1250.

[16] L. Tian et al., "Delay characteristics for directional and omni-directional channel in indoor open office and shopping mall environments at 28 GHz," in 2016 IEEE 27th Annual International Symposium on Personal, Indoor, and Mobile Radio Communications (PIMRC), Sept 2016, pp. 1-4.

[17] L. J. Greenstein et al., "Moment-method estimation of the Ricean K-factor," IEEE Communications Letters, vol. 3, no. 6, pp. 175-176, June 1999.

[18] L. Bernado et al., "Multi-dimensional K-factor analysis for V2V radio channels in open sub-urban street crossings," in IEEE 21st International Symposium on Personal Indoor and Mobile Radio Communications (PIMRC), 2010, pp. 58-63.

[19] M. K. Samimi et al., "28 GHz millimeter-wave ultrawideband small-scale fading models in wireless channels", in 2016 IEEE 83rd Vehicular Technology Conference (VTC Spring), May 2016, pp. 1C6.

[20] M. K. Samimi et al., "3-D millimeter-wave statistical channel model for 5G wireless system design," IEEE Transactions on Microwave Theory and Techniques, vol. 64, no. 7, pp. 2207-2225, July 2016.

[21] N. Czink et al., "A framework for automatic clustering of parametric MIMO channel data including path powers," in IEEE Vehicular Technology Conference, Sept 2006, pp. 1-5.

[22] C. Huang et al., "Cluster characteristics of wideband mimo channel in indoor hotspot scenario at 2.35 GHz," in 2009 IEEE 70th Vehicular Technology Conference Fall, Sept 2009, pp. 1-5.

[23] P. Tang et al., "Clustering in 3D MIMO channel: measurement-based results and improvements," in 2015 IEEE 82nd Vehicular Technology Conference (VTC2015-Fall), Sept 2015, pp. 1-6.

[24] B. H. Fleury et al., "Channel parameter estimation in mobile radio environments using the SAGE algorithm," IEEE Journal on Selected Areas in Communications, vol. 17, no. 3, pp. 434-450, Mar 1999.